

EFFECT OF TEMPERATURE AND LOADING RATE ON FRACTURE BEHAVIOUR OF CONCRETE SUBJECTED TO UNIAXIAL TENSION

V. Mechtcherine, H. Garrecht, and H.K. Hilsdorf,
Institute for Concrete Structures and Building Materials,
University of Karlsruhe, Germany

Abstract

The influence of temperature and loading rate on material response, in particular uniaxial tensile strength f_t , Young's modulus E_0 and fracture energy G_F as well as on the shape of the stress-strain and stress-crack opening relations was investigated. In addition, the roughness and fractal dimensions of the fracture surfaces were calculated in order to study failure mechanisms of concrete subjected to different test conditions.

1 Introduction

To analyse the deformation and crack formation behaviour of concrete structures under thermal loads a better knowledge of fracture properties of concrete subjected to such conditions is required.

In this, not only values of uniaxial tensile strength f_t , Young's modulus E_0 and fracture energy G_F are required, but also the shape of the total stress-deformation relation, necessary for a realistic prediction of the failure process has to be known (Roelfstra and Wittmann 1985). Uniaxial tensile tests are one of the most reliable tools to study these properties.

In recent years fracture surfaces became an object of comprehensive

research for better understanding of the energy consumption of a discrete crack (Mihashi and Umeoka 1993; Saouma and Barton 1994). In this project the fracture surfaces of the specimens were studied to interpret and explain the influence of temperature and loading rate on shape of stress-crack opening diagram.

The range of parameters covered in the experiments was obtained from numerical analysis of a concrete plate subjected to a thermal shock.

2 Preparation of specimens and test set-up

The composition of two types of concrete which were investigated is listed in Table 1. Their compressive strength at an age of 28 days was 53 N/mm² and 44 N/mm², respectively.

Table 1. Composition of the concretes (kg/m³)

w/c	cement	water	aggregate			superplasticizer
			0-2 mm	2-8 mm	8-16 mm	
0,45	424	182	516	654	551	8,5
0,6	318	190	543	688	580	1

Dog-bone shaped prisms with a gauge length of 250 mm were chosen to determine the uniaxial tensile strength f_t , modulus of elasticity E_0 , as well as the σ - ε -diagram for increasing stresses. Notched prisms were used to determine fracture energy G_F and the complete stress-deformation relation. Both

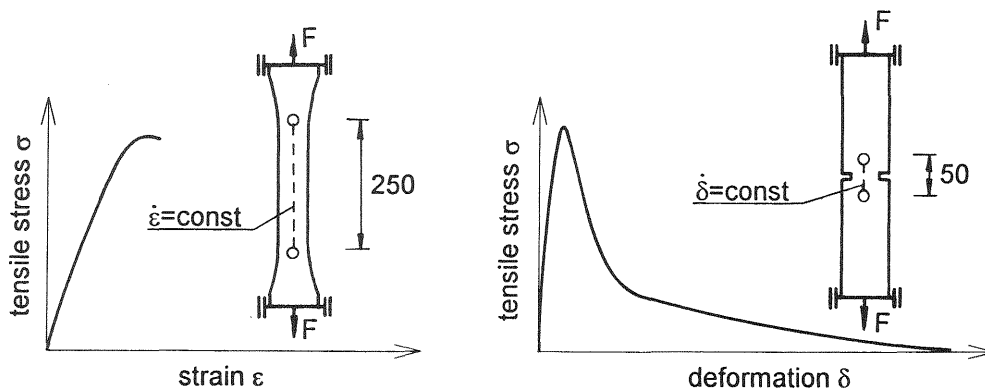


Fig. 1 Schematic view of the geometry of dog-bone (left) and notched (right) specimens with typical stress-deformation relations

types of specimens had the same effective cross-section 60*100 mm². A schematic view of the specimen geometries and typical stress-deformation relations are given in Fig. 1.

The specimens were cast horizontally in metal forms. After demoulding, the specimen were wrapped in a thin plastic sheet to which an aluminium foil was glued in order to protect the concrete against desiccation. Before testing at an age of 56 days the temperature of the specimens was adjusted to the required value in a constant environment chamber. During testing the specimens were kept in a specially constructed climatic box within the testing machine. To assure stable and possibly symmetrical crack propagation, the specimens were glued to stiff metal plates which in turn were firmly connected with the bearing platens of the testing machine. In the tests the deformation rate was controlled by means of the average signal of two LVDTs fixed to the specimens.

The uniaxial tension tests were performed at temperatures of 2 °C, 23 °C and 50 °C, respectively, with three different loading rates at each temperature as shown in Tables 2 and 3.

Table 2. Results of the uniaxial tension test on dog-bone specimens

w/c	θ, °C	ε̇, 1/s	n*	f _t , N/mm ²	E ₀ , N/mm ²	ε _{tu} , ‰
				average values (standart deviation)		
0.45	2	0.0001	3	5.3 (0.4)	39960 (840)	0.161 (0.012)
		0.00001	3	5.0 (0.3)	39180 (540)	0.158 (0.009)
		0.000001	4	4.8 (0.3)	38560 (630)	0.15 (0.006)
	23	0.0001	3	5.1 (0.4)	39730 (530)	0.158 (0.013)
		0.00001	4	4.5 (0.3)	38390 (450)	0.144 (0.007)
		0.000001	4	4.3 (0.3)	38150 (690)	0.145 (0.014)
	50	0.0001	3	3.8 (0.3)	36840 (250)	0.137 (0.011)
		0.00001	5	3.5 (0.1)	35660 (330)	0.138 (0.01)
		0.000001	5	3.2 (0.2)	34770 (300)	0.123 (0.008)
0.6	2	0.0001	4	4.9 (0.2)	38670 (580)	0.162 (0.015)
		0.00001	4	4.2 (0.4)	37620 (1100)	0.144 (0.015)
		0.000001	3	4.0 (0.1)	36360 (950)	0.142 (0.01)
	23	0.0001	3	4.5 (0.1)	38710 (970)	0.15 (0.006)
		0.00001	5	4.2 (0.1)	37080 (730)	0.149 (0.005)
		0.000001	5	3.8 (0.4)	36320 (1540)	0.13 (0.009)
	50	0.0001	3	3.7 (0.2)	37200 (910)	0.138 (0.017)
		0.00001	3	3.2 (0.2)	35860 (530)	0.125 (0.015)
		0.000001	3	2.8 (0.4)	34080 (660)	0.116 (0.026)

* Number of specimens

3 Experimental results

3.1 Results of uniaxial tension tests on dog-bone specimens

The ascending stress-strain relation for concrete subjected to uniaxial tension has a characteristic form as shown in the Fig. 1. Though linear-elastic at low stresses the stress-strain relation deviates from linearity at higher stresses due to microcrack formation, until it becomes horizontal at $\sigma = f_t$. With the particular test set-up employed stable crack propagation could not be achieved.

Acc. to Table 2, tensile strength f_t , modulus of elasticity E_0 and failure strain ϵ_{tu} at $\sigma = f_t$ decrease with increasing temperature for all strain rates investigated. An increase of strain rate results in an increase of f_t , E_0 and ϵ_{tu} .

3.2 Results of uniaxial tension tests on notched specimens

In these experiments also the descending branch of the σ - δ -relation could be determined up to nearly complete separation of the specimens into two parts because of the notches and of the reduction of the gauge length to 50 mm. For

Table 3. Results of the uniaxial tension tests on notched specimens

w/c	ϑ , °C	$\dot{\delta}$, mm/s	n*	f_{tn} , N/mm ²	G_F , N/m	l_{ch} , m
				average values (standart deviation)		
0.45	2	0.005	4	4.5 (0.3)	-	187.8
		0.0005	4	4.4 (0.3)	127.3 (23)	197.9
		0.00005	6	4.0 (0.3)	131.8 (19.2)	219.7
	23	0.005	3	4.0 (0.2)	139.8 (-)	216.9
		0.0005	7	3.8 (0.4)	129.9 (21.5)	251.8
		0.00005	3	3.5 (0.4)	110.45 (19.6)	226.8
	50	0.005	3	3.3 (0.0)	135.5 (8.8)	349.4
		0.0005	4	3.2 (0.1)	147.6 (20.8)	427.2
		0.00005	4	3.0 (0.4)	127.0 (15)	439.4
0.6	2	0.005	3	4.2 (0.3)	135.7 (28.1)	220.4
		0.0005	6	3.8 (0.3)	132.5 (13.0)	278.6
		0.00005	4	3.3 (0.2)	120.7 (22.9)	281.3
	23	0.005	3	3.8 (0.4)	145.0 (13.5)	280.9
		0.0005	5	3.2 (0.3)	130.1 (15.2)	272.2
		0.00005	5	2.9 (0.3)	140.8 (20.9)	350.4
	50	0.005	3	3.1 (0.3)	135.8 (18.3)	369.0
		0.0005	3	3.0 (0.3)	149.6 (6.4)	511.0
		0.00005	5	2.8 (0.3)	122.2 (13.9)	538.9

* Number of specimens

deformation rates of $5 \cdot 10^{-5}$ and $5 \cdot 10^{-4}$ mm/s the crack development stayed stable often up to a crack width of 0.5 mm, i.e. up to a nearly zero stress level.

At the higher rate of $\dot{\delta} = 5 \cdot 10^{-3}$ mm/s stable crack growth could rarely be achieved for $\delta > 0.1$ mm. Therefore, for the calculation of fracture energy G_F the σ - δ -relations were extrapolated to $\sigma = 0$ or $\delta = 0.5$ mm in cases where unstable crack growth occurred at $\delta < 0.5$ mm.

The values of tensile strength f_{tn} , fracture energy G_F and characteristic length $l_{ch} = \frac{G_F \cdot E_0}{f_t^2}$ are listed in Table 3. The fracture energy G_F was defined as the energy per unit area needed for complete separation of specimen into two parts and determined from the area under the σ - δ -relations for $0 < \delta < 0.5$.

Acc. to Table 3, no clear correlation between G_F and temperature or deformation rate was observed. This is in contrast to the data reported by Bazant and Prat (1988), who reported a decrease of G_F with increasing temperature.

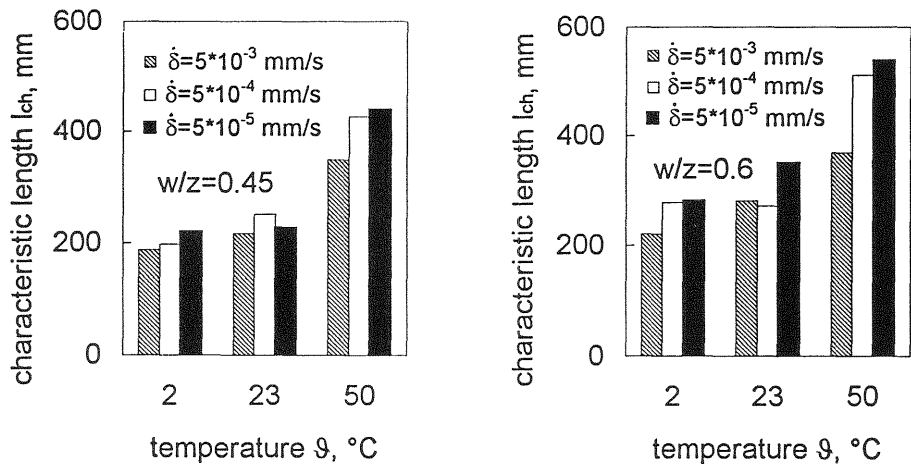


Fig. 2 Influence of temperature and deformation rate on the characteristic length of the concretes

The tensile strength f_{tn} shows a similar dependence on temperature and loading rate as the tensile strength f_t measured on dog-bone specimen, however $f_{tn} < f_t$, indicating a notch sensitivity of the concrete. The characteristic length l_{ch} increases with decreasing deformation rates and with rising temperature (Fig.2). This indicates a more ductile behaviour of concrete for such test conditions.

4 Quantification of the condition of the fracture surfaces

4.1 Measuring technique

To study the influence of temperature and deformation rate on crack propagation the fracture surfaces were measured using projected fringes techniques (Tiziani 1993). Height differences of the surface induce a lateral displacement of the projected strip pattern. The incorporation of geometrical data of the optical configuration then allows the contour information to be detected from the phase shift of the surface strip pattern at each surface location. The principle of projected fringes and a typical contour of a fracture surface are shown in Figs. 3 and 4. The measurement at the interval of 0.6 mm gives 100×166 mesh data for each fractured surface.

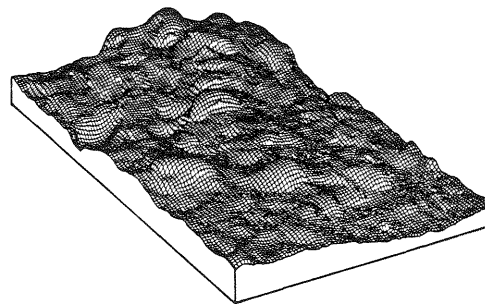
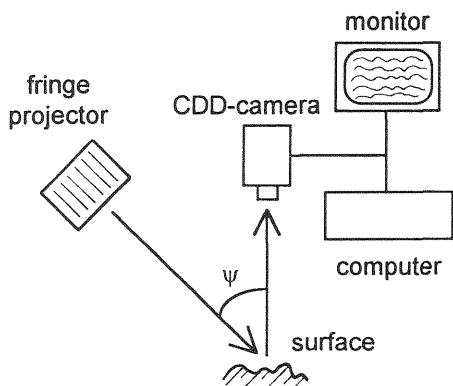


Fig. 3 Principle of the projected fringes technique

Fig. 4 A typical contour of fractured concrete surface

4.2 Determination of the roughness and fractal dimension

From the optical measurement data the roughness and the fractal dimensions of the surfaces were determined in order to quantify the condition of the fracture surfaces. The roughness of the fractured surface R_S was calculated as the surface area measured with 0.6 mm mesh size and divided by the projected area. The fractal dimensions were defined by two different methods.

Cube Counting Method (authors' nomenclature)

This method is an extension of the box counting method, successfully applied for studying fracture profiles by Saouma and Barton (1994). However, instead of boxes cubes of different sizes are generated over the 3D contour data. The number of cubes intersecting the surface N is plotted with respect to the

inverse of the cube size on a log-log scale. If a linear relationship is found, then the cube counting fractal dimension D_{CC} corresponds to the slope of the linear regression line (Fig. 5 left).

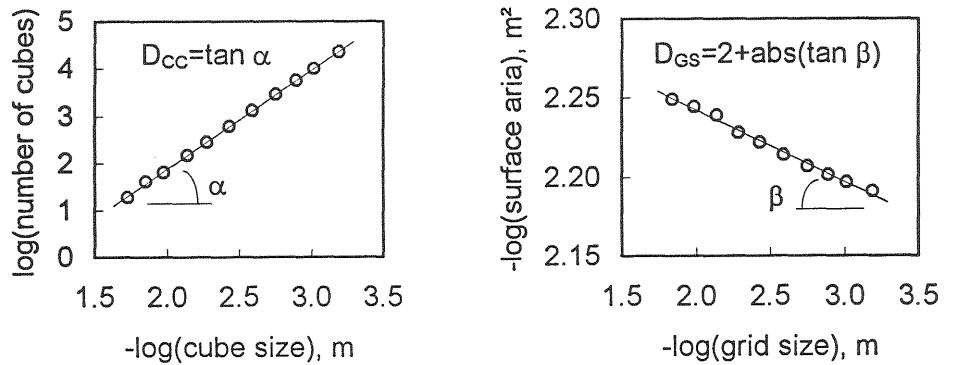


Fig. 5 Plots of cube counting method (left) and grid scaling method (right) applied to the fracture surface of a typical concrete specimen

Grid Scaling (authors' nomenclature)

For concrete fracture surfaces the grid scaling method was first applied by Mihashi and Umeoka (1993). This method is based on the fact that the measured surface area increases as the grid size decreases. The plot of the log of the measured surface area and log of the grid size gives the negative value of fractal increment = $\tan \beta$ (Fig. 5 right). The grid scaling fractal dimension D_{GS} can be calculated by adding this value to the dimension of a plane = 2.

Table 4. Roughness and fractal dimensions of concrete fracture surfaces

w/c	$\vartheta, ^\circ\text{C}$	$\dot{\delta}, \text{mm/s}$	$n^1)$	Roughness R_s		Fractal Dimension determined by			
						Cube Counting		Grid Scaling	
				$m(R_s)^2)$	$\sigma(R_s)^2)$	$m(D_{CC})$	$\sigma(D_{CC})$	$m(D_{GS})$	$\sigma(D_{GS})$
0.6	23	$5 \cdot 10^{-3}$	3	1.192	0.013	2.134	0.012	2.046	0.003
		$5 \cdot 10^{-5}$	3	1.204	0.015	2.150	0.014	2.05	0.003
0.45	2	$5 \cdot 10^{-4}$	3	1.169	0.011	2.104	0.011	2.042	0.002
	50		3	1.205	0.006	2.129	0.01	2.048	0.002

- 1) Number of analysed surfaces
- 2) m = average; σ = standard deviation

To study the influence of temperature on crack propagation the fractured surfaces of the concrete specimens with $w/c=0.45$ tested at 2 °C and 50 °C were determined. The influence of the deformation rate on the fracture surfaces was studied for the specimens with $w/c=0.6$ tested with $\dot{\delta} = 5 \cdot 10^{-3}$ and $5 \cdot 10^{-5}$ mm/s. Table 4 gives the results of the calculations.

5 Discussion of the experimental results

5.1 Influence of the temperature

The decrease of the tensile strengths f_t and f_m as well as of Young's modulus E_0 at high temperatures is due to the weakening of the van der Waals bond in the cement gel structure and in the cement gel - aggregate interfaces.

Fig. 6 shows the influence of temperature on the shape of the stress - crack opening relation. The area under the initial part of the σ - w -relation increases at lower temperatures indicating an increase of energy consumption for the formation and propagation of narrow cracks with decreasing temperature.

For larger crack widths this trend reverses, and the σ - w -relations measured at higher temperature are above those measured at the lower temperature. The higher roughness and the higher fractal dimensions of the fracture surfaces of the specimens tested at 50 °C (Table 4) give an explanation for this phenomenon.

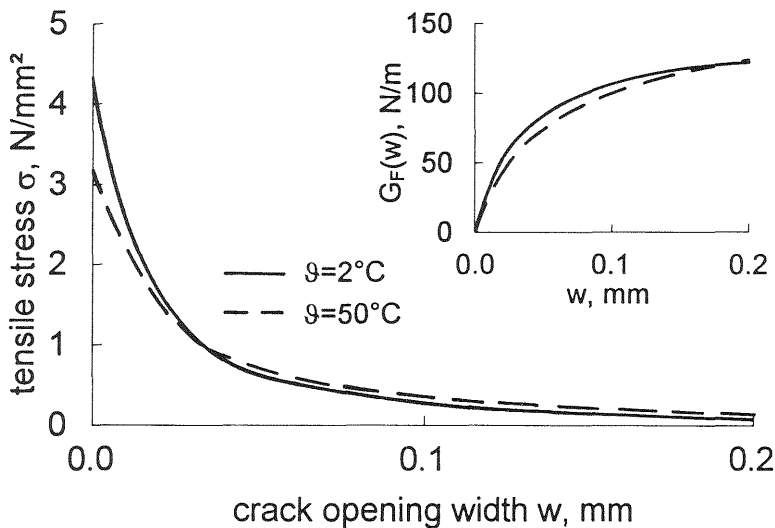


Fig. 6 Influence of temperature on the form of the σ - w -relation; average curves for $\dot{\delta} = 5 \cdot 10^{-4}$ mm/s; $w/c=0.45$

As a result fracture energy does not change significantly with a change of temperature in the investigated temperature range, provided G_F is determined from σ - w -relations up to $\sigma \sim 0$.

5.2 Influence of the deformation rate

Calculations made by Bachmann (1993) showed that an increase of deformation rate leads to the formation of a larger number of smaller microcracks in the concrete. As a consequence both f_t and ε_{tu} increase with increasing deformation rate.

As shown in Fig. 7 for small values of w the σ - w -relation for the high strain rate is above that for the lower strain rate, whereas for large crack openings this trend reverses. This is in agreement with the conclusion of Wittmann et al. (1987), that „at very low rates of loading ... the widening of the fracture process zone becomes more important...“. Also the data given in Table 4 show a slight, however significant, increase in roughness and fractal dimension at the fracture surfaces with decreasing deformation rate.

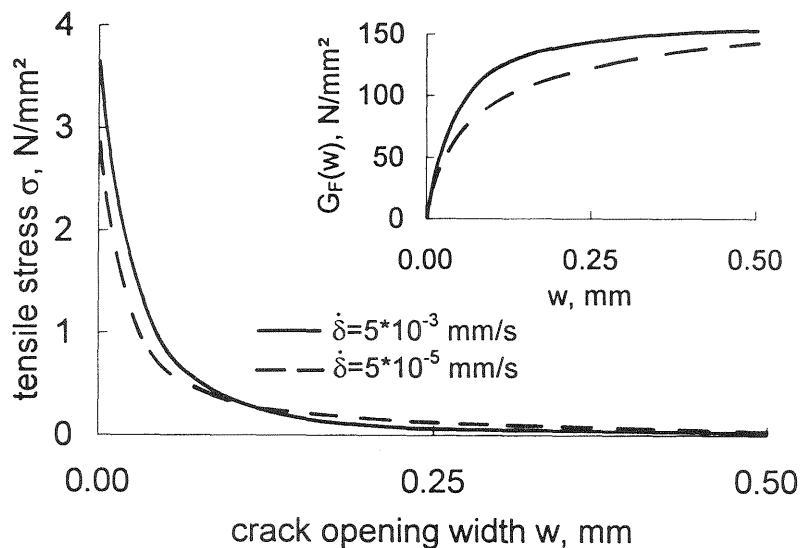


Fig. 7 Influence of deformation rate on the form of the σ - w -relation; average curves measured at 23 °C; $w/c=0.6$

6 Conclusions

1. The uniaxial tensile strength f_t , the Young's modulus E_0 and the fracture strain ε_{tu} increase with increasing deformation rate and decreasing temperature.

2. The σ -w-relation becomes steeper with decreasing temperature and increasing deformation rate.
3. The roughness of concrete fracture surfaces measured with a grid size of 0.6 mm as well as the fractal dimensions of the fracture surfaces increase with increasing temperature and decreasing deformation rate.
4. No clear correlation between fracture energy G_F and temperature or deformation rate and was observed in this investigation.
5. The characteristic length l_{ch} decreases with increasing deformation rate and decreasing temperature, i.e. the fracture becomes more brittle.

Acknowledgements

The measurements on fractured surfaces were performed by Th. Wolf and B. Gutmann, Institute of Mechanical Process Engineering and Mechanics, University of Karlsruhe. Their contribution is gratefully acknowledged.

7 References

- Bachmann, H. (1993) Die Massenträgheit in einem Pseudo-Stoffgesetz für Beton bei schneller Zugbeanspruchung. **Schriftenreihe des Instituts für Massivbau und Baustofftechnologie**, Heft 19, Universität Karlsruhe.
- Bazant, Z.P. and Prat, P.C. (1988) Effect of temperature and humidity on fracture energy of concrete. **ACI Mater. J.**, 84, 262-271.
- Mihashi, H. and Umeoka, T. (1993) Fracture properties of fiber reinforced cementitious composite materials. **Proc. 3rd Japan International SAMPE Symposium**, 224-229.
- Roelfstra, P.E. and Wittmann, F. H. (1985) Some aspects of the concept of total fracture energy. **Vorträge der 17. Sitzung des Arbeitskreises Bruchvorgänge**, Ed. Deutscher Verband für Materialprüfung, Berlin.
- Saouma, V.E. and Barton, C. (1994) Fractals, fractures, and size effects in concrete. **Journal of Engineering Mechanics, ASCE**, 120, 835-854.
- Tiziani, H.J. (1993) High precision optical surface topometry. **Ber. Bunsenges. Phys. Chem.**, 97, No. 12, 1664-1673.
- Wittmann, F.H., Roelfstra, P.E., Mihashi, H., Huang, Y.-Y., Zhang, X.-H. and Nomura, N. (1987) Influence of age of loading, water-cement ratio and rate of loading on fracture energy of concrete, **Materials and Structures**, 20, 103-110.